

The influence of Kola Peninsula, continental European and marine sources on the number concentrations and scattering coefficients of the atmospheric aerosol in Finnish Lapland

Aki Virkkula¹⁾, Risto E. Hillamo²⁾, Veli-Matti Kerminen²⁾ and
Andreas Stohl³⁾

¹⁾ *Finnish Meteorological Institute, Air Quality Department, Sahaajankatu 20E, FIN-00810 Helsinki, Finland; Present address: Joint Research Centre, Environment Institute, I-21020 Ispra, Italy*

²⁾ *Finnish Meteorological Institute, Air Quality Department, Sahaajankatu 20E, FIN-00810 Helsinki, Finland*

³⁾ *Institute for Meteorology and Physics, University of Agriculture, Forestry, and Renewable Natural Resources, Türkenschanzstrasse 18, A-1180 Vienna, Austria; Present address: Lehrstuhl für Bioklimatologie und Immissionsforschung Ludwig-Maximilians-Universität München Am Hochanger 13, D-85354 Freising-Weihenstephan, Germany*

Virkkula, A., Hillamo, R. E., Kerminen, V.-M. & Stohl, A. 1997. The influence of Kola Peninsula, continental European and marine sources on the number concentrations and scattering coefficients of the atmospheric aerosol in Finnish Lapland. *Boreal Env. Res.* 2: 317–336. ISSN 1239-6095

Atmospheric aerosols were measured at Sevettijärvi in Finnish Lapland in 1992–1995. The variation of aerosol concentrations in different air masses has been examined. In polluted air from the Kola peninsula particle number concentrations were often $> 10\,000\text{ cm}^{-3}$. In marine and continental air mean particle number concentrations were $60\text{--}350\text{ cm}^{-3}$ and $200\text{--}1\,120\text{ cm}^{-3}$, respectively. They were lower in air from the Arctic Sea than in air from the Norwegian Sea. This is explained by the difference in the natural sulphur emissions and resulting particle production between these two areas. In marine air, the mean scattering coefficient (σ_{sp}) at 550 nm was $2\text{--}8 \times 10^{-6}\text{ m}^{-1}$, in continental air $2\text{--}3 \times 10^{-5}\text{ m}^{-1}$, and in pollution plumes $< 9 \times 10^{-5}\text{ m}^{-1}$. The mean backscatter fraction in marine air, continental air and in pollution plumes was 0.13, 0.11, 0.10, respectively. The impact of the air pollution sources in northern Siberia was detected despite the vicinity of Kola peninsula pollution sources.

Introduction

In the Arctic, ground-based measurements of atmospheric aerosols have been conducted in many locations including: Alert and Barrow in Alaska (e.g., Raatz and Shaw 1984, Barrie *et al.* 1989, Bodhaine 1983, Bodhaine 1989, Djupström *et al.* 1993), Greenland (e.g., Heidam *et al.* 1993, Hillamo *et al.* 1993, Jaffrezo and Davidson 1993), and Ny Ålesund in Spitsbergen (e.g., Heintzenberg 1980, Heintzenberg *et al.* 1981, Pacyna *et al.* 1985, Covert and Heintzenberg 1993, Djupström *et al.* 1993, Heintzenberg and Leck 1994, Beine *et al.* 1996). Airborne aerosol measurements over the European Arctic were also conducted, e.g., by Ottar *et al.* (1986) and Heintzenberg *et al.* (1991).

On the European mainland, the Arctic includes the northern parts of Norway, Sweden and Finland, and the northwestern parts of Russia. In these regions, continuous ground-based aerosol measurements have been carried out as part of existing monitoring programs (e.g., EMEP), and consist mainly of filter measurements. Thus, data on particle number concentrations and scattering coefficients from the continental European Arctic are scarce.

In the European Arctic, the Kola Peninsula industrial areas are by far the largest source of sulphur aerosols. Practically all sulphur emissions north of the Arctic Circle originate from two well-defined regions: the Norilsk area in Siberia (2.2 Tg yr⁻¹ of SO₂) and the Kola Peninsula (0.6 Tg yr⁻¹ of SO₂) (Tuovinen *et al.* 1993). The sources in the Kola Peninsula contribute almost 20% to the global anthropogenic sulphur emissions north of 60° N. The SO₂ emissions from the non-ferrous smelters in Nikel and Zapolyarnyj in the Kola Peninsula, close to the Norwegian border, amount to 0.26 Tg yr⁻¹, which is twice the amount emitted from the whole of Finland (Tuovinen *et al.* 1993).

A station for measuring atmospheric aerosols and trace gases was founded at Sevetijärvi (69°35' N, 28°50' E, 130 m a.s.l.) (Fig. 1) by the Finnish Meteorological Institute (FMI) and the Finnish Forest Research Institute in summer 1991. The original goal was to give information of air quality for the Lapland Forest Damage Project, a multidisciplinary effort to determine the effects of Kola emissions on the health of forests in Lapland (Tikkanen and Niemelä 1995). Sevetijärvi measurements were previously presented by, e.g., Djupström-Fridell (1995),

Kerminen *et al.* (1997), Virkkula *et al.* (1995 and 1996), Virkkula and Hillamo (1995), and Virkkula (1997).

The aim of this paper is to study how the relatively closely-located large pollution source in the Kola peninsula affects the aerosol measurements at the site. We examine whether aerosol concentrations reach as low levels as at more distant Arctic background stations. In the papers quoted above dealing with Sevetijärvi measurements, criteria for classifying air in different air masses — marine, continental and pollution plumes — was not clearly established. In the present paper we therefore try to find classification criteria for all subsequent analyses of Sevetijärvi measurements, both for gas and aerosol monitoring and for aerosol sampling. The possible criteria are based on particle number concentration and light scattering coefficient, which are roughly a measure of submicron aerosol mass, sulphur dioxide concentration, wind direction, and air mass trajectories.

Methods

Instrumentation

Particle counters

Condensation nuclei (CN) concentrations have been measured since March 1992 using a TSI model 3760/7610 CPC, which detects particles that have a diameter (D_p) larger than 14 nm. The coincidence error, approximately 6% at 10 000 cm⁻³, has to be taken into account especially during pollution episodes from Nikel and it has been corrected. The CPC flow is controlled by a critical orifice inside the instrument. The sample flow rate is monitored using a 5-cm-long venturi meter which is inserted between the connection to the main flow and the counter. The pressure drop over the venturi meter, 25 Pa, is checked every four days. In addition, the flow rate is measured with a Gilibrator flow meter after maintenance (5–6 times a year). The critical orifices are either cleaned or changed if there are signs of a decreasing flow rate. The CPC butanol reservoir is refilled once a day using an automatic valve. The data are stored in a computer as five-minute averages. The counter is calibrated twice a year by bringing it to the FMI aerosol laboratory in

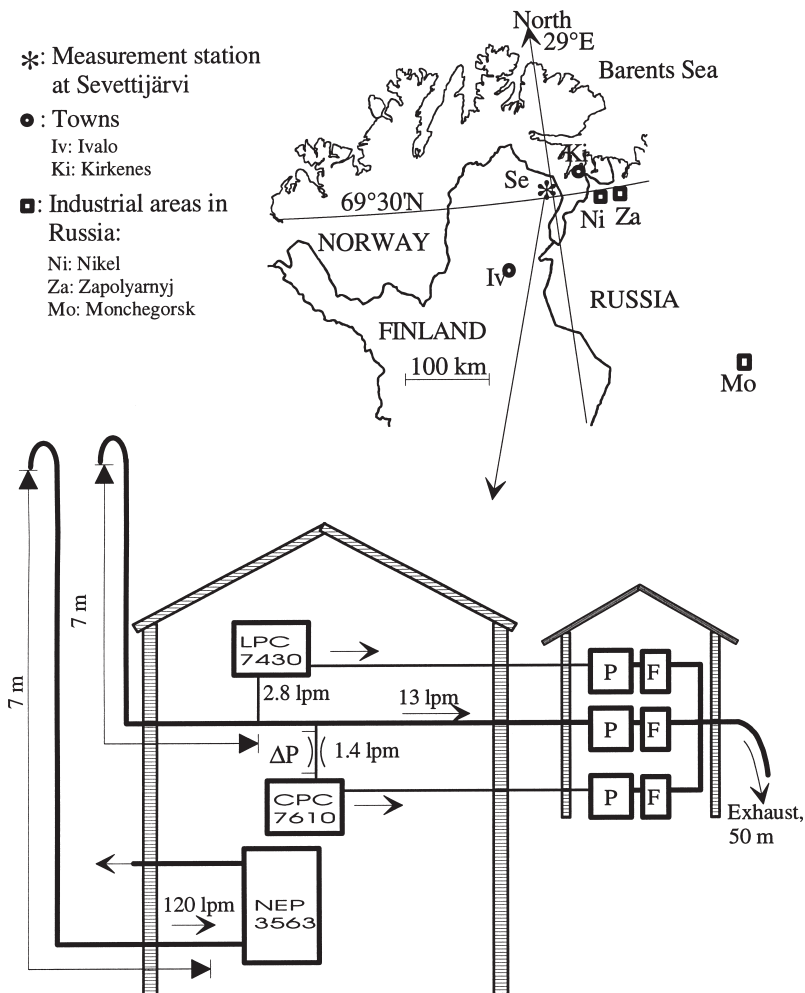


Fig. 1. Top: Location of the Sevetijärvi measurement station. Bottom: schematic flow and instrument arrangement at the station.

Helsinki, and comparing it with a TSI 3025 CPC and with a TSI 3760 CPC.

Since March 1994, particle number concentrations have been monitored using also a TSI model 7430 laser particle counter (LPC) which counts particles in two size channels, $0.3 < D_p < 0.5 \mu\text{m}$ and $D_p > 0.5 \mu\text{m}$. These sizes cover the accumulation mode of aerosol mass size distribution. The data are stored in a computer as five-minute averages. The LPC was calibrated by TSI prior to shipping to Finland, and the first place it was used was the Sevetijärvi station.

Nephelometer

The aerosol scattering extinction coefficient, σ_{sp} , and backscattering coefficient, σ_{bsp} , were meas-

ured using a TSI model 3563 three-wavelength nephelometer ($\lambda = 450 \text{ nm}, 550 \text{ nm}, \text{ and } 700 \text{ nm}$). The instrument is described in detail by Bodhaine *et al.* (1991) and by Anderson *et al.* (1996). Calibration of the nephelometer, which is accomplished by filling it with CO_2 , was carried out twice: after the first installation of the instrument in December 1994, and in April 1995. The nephelometer data lasts until June 30 because at the beginning of July 1995 there was an instrument failure and it was removed from the station for service. The internal heater of the device kept the relative humidity (RH) of the sample air low: the mean $\text{RH} \pm \text{STD}$ of the hourly mean values during the 7 month period was $18 \pm 8\%$, the maximum hourly mean RH was 45%. Thus, the scattering coefficients are a measure of dry aerosol. The sample temperature t_s followed the ambient

air temperature t_a according to $t_s = (0.487 \pm 0.005) \times t_a + (14.55 \pm 0.04)^\circ\text{C}$, with $r^2 = 0.67$. The sample flow is provided by the internal blower of the instrument. According to Anderson *et al.* (1996), the instrument's detection limits for 5-min averages are 0.2 and 0.1 M m^{-1} for total scatter and backscatter, respectively, at 550 nm. In this work the averaging time was set to 5 minutes. The data were stored in a computer as 15 min averages.

Sample flow system

The sample flow system is shown schematically in Fig. 1. There is a common inlet tube for the CPC and LPC. The nephelometer has an inlet tube of its own. Both of the inlet tubes are made of stainless steel. They are located one meter apart and they sample air at the same height, approximately 4.5 m above the ground. Including the part of the tubes which are inside the building, they are approximately 7 meters long. The LPC/CPC inlet tube has an inner diameter of 18 mm, and that of the nephelometer has an inner diameter of 25 mm. The particle losses in the inlets and sampling tubes were estimated using the equations given by Brockman (1993). The total transport efficiency of the system has been calculated according to:

$$\eta_{\text{total}}(D_p, \rho_p, D_t, L, U_o, U, \theta, T, p) = \eta_{\text{inlet}} \times \eta_{\text{transport}} = \eta_{\text{asp, inlet}} \eta_{\text{trans, inlet}} \times \eta_{\text{diff}} \eta_{\text{bend}} \eta_{\text{asp, main-LPC/CPC}} \eta_{\text{cont, CPC}} \quad (1)$$

where D_p = particle diameter, ρ_p = particle density, D_t = tube diameter, L = tube length, U_o = ambient air velocity, U = sample flow velocity, θ = angle between sample flow and ambient air velocity, T = temperature, p = pressure, $\eta_{\text{asp, inlet}}$ = aspiration efficiency of the inlet, $\eta_{\text{trans, inlet}}$ = transmission efficiency for inertia in the inlet; η_{diff} = transmission efficiency due to diffusion in the tubes, η_{bend} = transmission

efficiency due to the 90° bends in the tubes, $\eta_{\text{asp, main-LPC/CPC}}$ = aspiration efficiency of the main tube to CPC or LPC sample flow tubes, $\eta_{\text{cont, CPC}}$ = transmission efficiency of the CPC venturi meter contraction. The transport efficiencies were calculated at 273 K and 1013 hPa for particles with a density of 1.7 g cm^{-3} (model aerosol by Seinfeld 1986). The ambient air velocity affects the inlet transmission efficiency, η_{inlet} , and therefore the calculations were done three times: using the mean wind speed \pm standard deviation. The results are presented in Table 1 which shows the diameters of particles which are transported at 90% and 50% efficiency (D_{90} and D_{50}). The inlet efficiency dominates the total transport efficiency. During strong wind the D_{50} and D_{90} values of the LPC and CPC inlet tubing goes down to 2.6 and 0.5 μm .

According to size distribution measurements (e.g., Heintzenberg 1980), the highest number concentrations are typically at diameters around 0.1–0.2 μm . Therefore the CPC measurements are not drastically affected by wind speed variations. The effect of the venturi meter contraction is important only at diameters larger than 3 μm which on the other hand are not important for the CPC measurements. The LPC measures particles in two size channels, with $0.3 < D_p < 0.5 \mu\text{m}$ and $D_p > 0.5 \mu\text{m}$, and thus especially the upper channel concentrations are underestimated during strong wind. The scattering coefficient measurements are done at wavelengths 0.45, 0.55, and 0.7 μm and the scattering is most efficient when the size of the particle is close to the wavelength of the scattered light. Therefore, according to Table 1 wind speed variations do not practically have any effect on the nephelometer measurements. This is due to the high velocity at the inlet of the nephelometer.

Gas measurements

Ozone, sulphur dioxide, nitrogen dioxide, nitrate radical, and water vapour are measured using a commercial Differential Optical Absorption Spectrometer (DOAS), model AR 500, manufactured by Opsis AB, Lund, Sweden. The DOAS has been calibrated for SO_2 and NO_2 three or four times a year, using two calibration cells of known lengths and three different concentrations of SO_2 or NO_2 , delivered by AGA AB, mixed in N_2 , and pure N_2 , giving seven calibration points. In addi-

Table 1. D_{50} and D_{90} -values (μm) of the transport efficiency curves of the various inlet tubes at mean and mean \pm STD (4 \pm 3 m/s) wind speeds (V).

V (m/s)	CPC		LPC		Nephelometer	
	D_{90}	D_{50}	D_{90}	D_{50}	D_{90}	D_{50}
1	2.8	6.3	8.4	14.2	5.1	13
4	1.5	3.8	1.5	6.2	3.9	9.8
7	0.5	2.6	0.5	2.8	2.2	6.7

tion, an intercomparison between a conventional SO₂ monitor (TEI 43S) and the DOAS was carried out from March 2 to June 17, 1995. The corresponding regression line was: $[\text{SO}_2]^{\text{DOAS}} = (1.11 \pm 0.01) \times [\text{SO}_2]^{\text{TEI}} + (0.5 \pm 0.1) \mu\text{g m}^{-3}$, ($r^2 = 0.95$, $N = 2506$) at light levels above 17%. There was a zero-point drift in the TEI monitor, though, which explains part of the offset in the regression line. DOAS SO₂ measurements have not been corrected according to the above relationship. With the programmed two-minute integration time and 1 021 m path length the quantitative detection limit ($3 \times \text{noise}$) for SO₂ is approximately 0.3–0.4 $\mu\text{g m}^{-3}$ at good visibility, but it rises with reducing visibility. The relationship between DOAS detection limit and visibility has been discussed by Virkkula (1997), who showed that at Sevettijärvi approximately 3% of the measurements have been rejected due to reduced visibility. The data were stored as 15-minute averages in a computer.

Weather data

Temperature, pressure, relative humidity, total radiation and rain intensity are monitored two meters above the ground, and wind at a height of 7.5 m above the ground. The data are stored as five-minute averages in a computer. Using the measured temperature and pressure, the concentrations given by the DOAS are transformed to give values at 1 013 mbar and 273 K.

Trajectories

Three or four three-dimensional 96-hour back-trajectories arriving at ground level, at 950 hPa, and at 900 hPa level, were calculated for each day. For the period from January 1992 to June 1994, a total of 4 512 trajectories for each level were calculated. Most trajectories were calculated using the TRADOS model of FMI. An early version of the model was presented by Valkama and Rossi (1992). The present version of the model calculates trajectories using the numerical 6-hour forecasts of the Finnish version of the Nordic HIRLAM (High Resolution Limited Area Model) weather prediction model (Salonja 1993, Valkama and Salonja 1993, Valkama *et al.* 1995). The grid resolution of the HIRLAM fields is 55 km \times 55 km. TRADOS uses seven post-processed lev-

els of the 31 HIRLAM pressure levels.

For the year 1992, three-dimensional trajectories were calculated using the FLEXTRA trajectory model described in detail by Stohl *et al.* (1995). FLEXTRA is based on analysed model-level wind fields of the T213 L31 weather prediction model of the European Centre for Medium-Range Weather Forecasts (ECMWF). Analysed and 3-h forecast wind fields were available every 3 h at a 0.5 \times 0.5 degree resolution.

Data presentation

Temporal variation and comparison with other Arctic stations

Time series of hourly-mean particle number concentrations, scattering coefficient (for clarity only at $\lambda = 550 \text{ nm}$), the hemispheric backscattering ratio R ($= \sigma_{\text{bsp}}/\sigma_{\text{sp}}$) and sulphur dioxide concentrations during 1992–1995 are plotted in Fig. 2, and the corresponding monthly geometric means in Fig. 3. The monthly geometric means of the Ångström exponent, α_{12} , are also presented in Fig. 3. The explanation of α will be given below. Statistical properties of the measured quantities are presented in Table 2 and Fig. 4. In the table the variation of the values is expressed as standard deviations, and also as percentiles because the standard deviation of most properties is so large that mean – std would be negative and thus no estimation of the low range values can be calculated so.

CN concentrations varied from below 100 cm^{-3} to over 10 000 cm^{-3} . The mean and variability of CN concentrations at Sevettijärvi are clearly higher than at Ny Ålesund, Spitsbergen and at Barrow, Alaska (Fig. 4). The mean and the standard deviation of the logarithm of CN concentrations at Barrow in 1976–1986 was 2.29 ± 0.30 (Bodhaine 1989) and at Sevettijärvi 2.84 ± 0.45 . At Spitsbergen mean CN concentrations \pm std were $117 \pm 94 \text{ cm}^{-3}$ during a measurement campaign between February 19 to May 31, 1994 (Beine *et al.* 1996). At Sevettijärvi an increase in CN concentrations was observed when the polar night turned to spring in the winters of 1992–93 and 1994–95. The geometric mean CN concentration in December 1992 and 1994 was approximately 300 cm^{-3} , whereas in March and April 1993 and 1995 it was approximately 1 000 cm^{-3} . In the winter of 1993–94 a similar spring increase was not

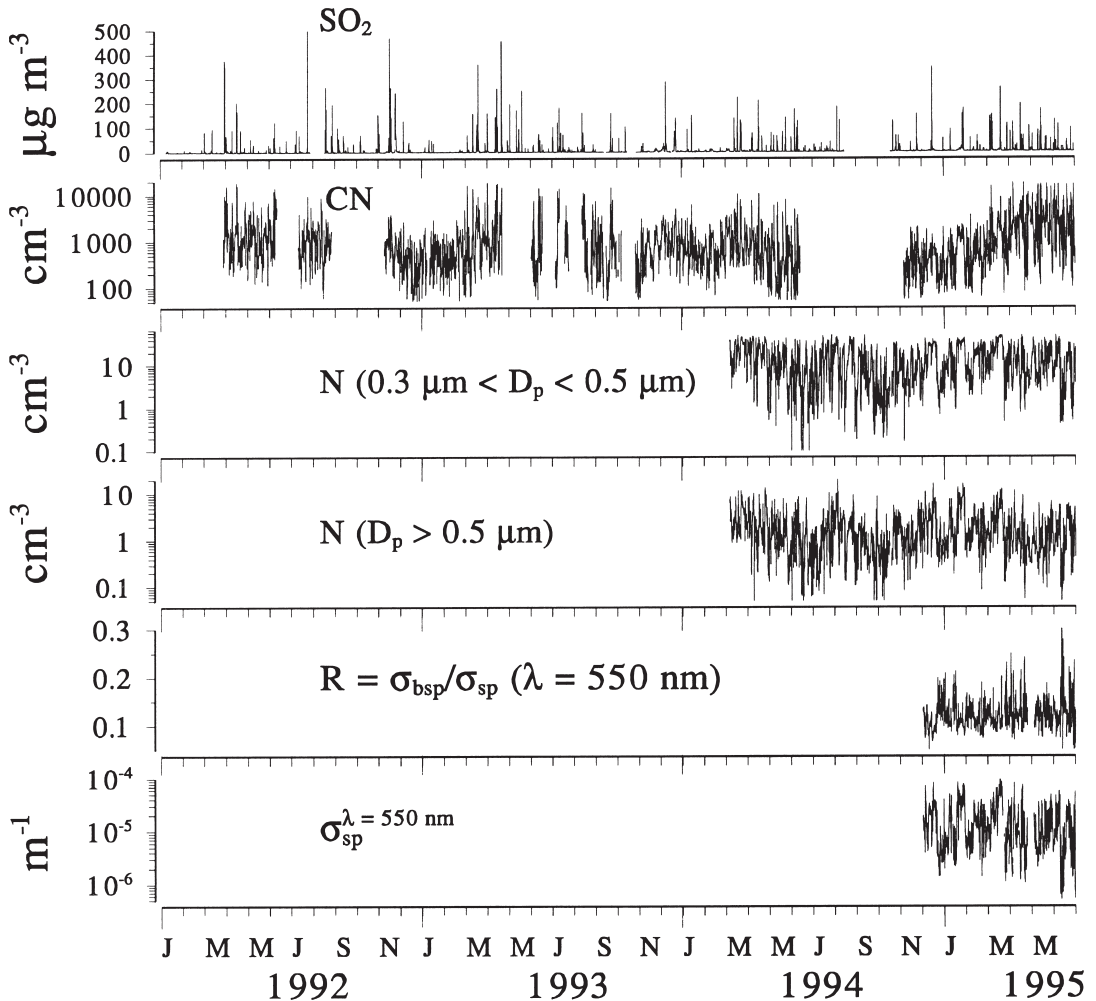


Fig. 2. Hourly mean SO_2 concentrations, particle number concentrations, scattering coefficients and backscatter fractions at $\lambda = 550$ nm, measured at Sevettijärvi in 1992–1995.

so evident. The spring-time CN peak is found at many other Arctic sites. In addition, a more complex seasonal variation was reported, e.g., at Barrow by Bodhaine (1989) and at Spitsbergen by Heintzenberg and Leck (1994). They observed semi-annual cycles with two maxima, one in late winter and another in the summer months and minima in May and October–November. The summer peak is probably due to biogenic processes in the ocean (Heintzenberg and Leck 1994, Bodhaine 1989), and at Barrow also possibly in the tundra (Bodhaine 1989). The Sevettijärvi CN data have discontinuities that make the analysis of annual cycles incomplete. The discontinuities in 1992 and 1993 are due to breaks in the computer system storing the data. In August

1994, the CPC sample-flow focusing nozzle became clogged and the CPC was removed from the station for repair. The CN data for summer 1994 were therefore discarded. The CPC was reinstalled in November 1994. The discontinuities took place in summer, and therefore there is little data to give information about a possible summer maximum.

The LPC-data in the smaller-particle ($0.3 \mu\text{m} < D_p < 0.5 \mu\text{m}$) channel deviates clearly from the log-normal distribution, a straight line on the axes scales used in Fig. 4. Approximately 10% of the concentrations were higher than the saturation point, 35.3 cm^{-3} . If it is assumed that the distribution is log-normal, the number concentration in this range would be several hundreds of particles cm^{-3} . Because of

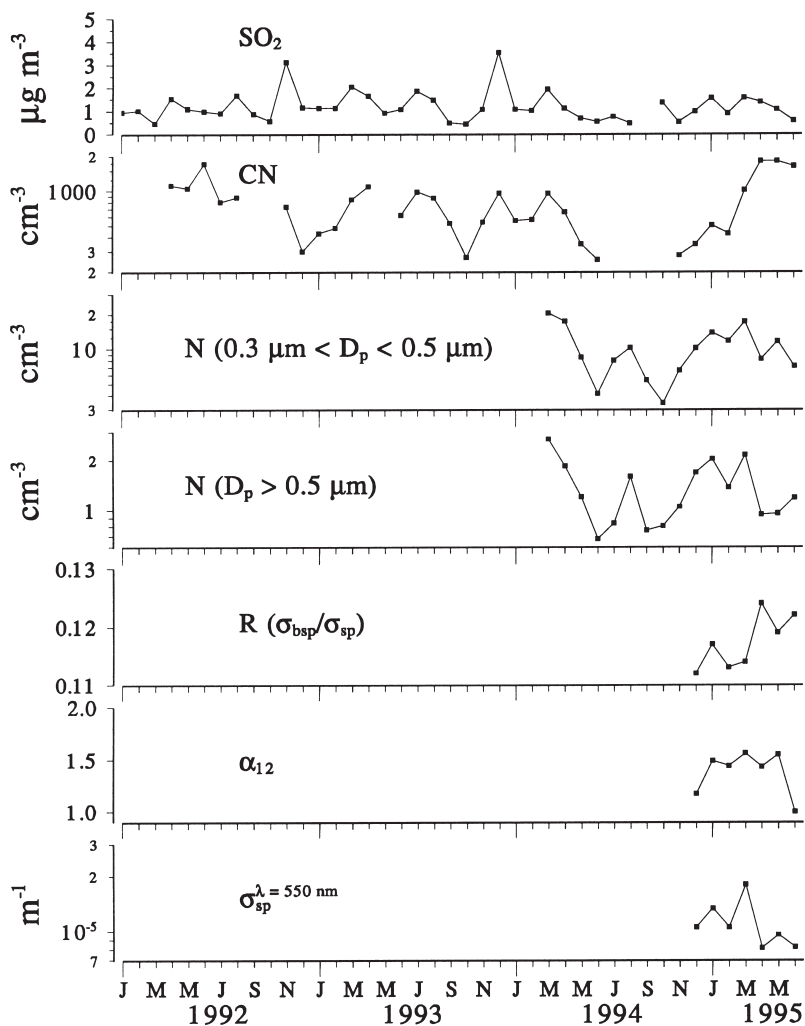


Fig. 3. Monthly geometric mean SO_2 concentrations, particle number concentrations, scattering coefficients and backscatter fractions at $\lambda = 550 \text{ nm}$, and Ångström exponents α_{12} , measured at Sevettijärvi in 1992–1995.

the saturation, LPC smaller-particle channel results will not be discussed further. The upper end of the total scattering data also deviates from a log-normal distribution. There is no obvious explanation for this. If there is some instrumental reason for the deviation, the highest scattering coefficients are higher than those measured.

The evolution of SO_2 concentration is plotted on a linear scale to illustrate the typical peak-like nature of pollution episodes from Nikel. The concentration varies strongly. Most of the time it is $< 1 \mu\text{g cm}^{-3}$ but when the air comes from Nikel, SO_2 levels frequently exceed $100 \mu\text{g m}^{-3}$. During 1992–1995, episodes with SO_2 concentrations above $100 \mu\text{g m}^{-3}$ occurred approximately every two weeks. Their duration usually varied only from two to four hours, but occasionally they lasted up to two days. The high-

est daily mean SO_2 concentration during 1992–1995 was $114 \mu\text{g m}^{-3}$. The variability of the particle parameters is not as large as that of SO_2 , which shows that the pollution episodes from nearby Nikel have a larger effect on the SO_2 concentrations than on particle concentrations. This is expected due to a limited gas-to-particle conversion of SO_2 during the transport from the Kola Peninsula to Sevettijärvi. More than 60% of the SO_2 concentrations were low (i.e., $< 1 \mu\text{g m}^{-3}$), and 10% were close to or even less than the detection limit of $0.3 \mu\text{g m}^{-3}$. Concentrations between 1 and $10 \mu\text{g m}^{-3}$, 31% of the hourly means, were usually detected in air masses from continental Europe. All concentrations above $30 \mu\text{g m}^{-3}$, constituting approximately 4% of the hourly means, were detected during pollution episodes from Nikel.

The scattering coefficient σ_{sp} follows the varia-

tions in particle concentrations in the $D_p > 0.3 \mu\text{m}$ size range. This is expected, since light scattering is strongest at wavelengths close to the particle diameter. It was previously shown by Virkkula and Hillamo (1995) that the correlation between CN concentration and $\sigma_{\text{sp}}(550\text{nm})$ is low, but high between the number concentration in the accumulation-mode of the mass size distribution ($D_p > 0.3 \mu\text{m}$) and $\sigma_{\text{sp}}(550 \text{ nm})$. The monthly geometric mean scattering coefficient reached a maximum in March ($\sigma_{\text{sp}}(550) = 1.8 \times 10^{-5} \text{ m}^{-1}$), and a minimum in April ($\sigma_{\text{sp}}(550) = 8.1 \times 10^{-6} \text{ m}^{-1}$). The variation during the measurement period is not as large as at Barrow and Spitsbergen, where the annual cycle of σ_{sp} shows a change by a factor of 10. At Barrow, the monthly geometric mean $\sigma_{\text{sp}}(550)$ in 1976 to 1986 had a maximum in March ($> 1 \times 10^{-5} \text{ m}^{-1}$) and a minimum in July ($< 2 \times 10^{-6} \text{ m}^{-1}$) (Bodhaine 1989). At Spitsbergen, at sea level, the average $\sigma_{\text{sp}}(550)$ in 1979 to 1990 was $1.6 \times 10^{-5} \text{ m}^{-1}$ in winter and $1.5 \times 10^{-6} \text{ m}^{-1}$ in summer (Heintzenberg and Leck 1994) and during a measurement campaign between February 19 to May 31, 1994, $(5 \pm 3.9) \times 10^{-6} \text{ m}^{-1}$ (Beine *et al.* 1996). The mean scattering coefficients at Sevettijärvi are generally higher than at Spitsbergen and at Barrow (Fig. 4). An exception are the backscattering coefficients, when they are compared with the 19-day means at Ny Ålesund in spring 1979.

When the light scattering coefficient is measured at various wavelengths, the particle size distribution that caused the observed light scattering

can be solved. For instance, Heintzenberg (1980) analysed his scattering coefficient and particle number concentration data from Spitsbergen by solving the integral equation $S = \int K(D_p)N(D_p)dD_p$, where S represents the measured integral optical properties. $K(D_p)$ is the corresponding kernel of the integral equation and describes the optical effect of a particle with diameter D_p . An inversion algorithm returns the solution $N(D_p)$, the number size distribution of the particles. However, the calculation of the kernels requires information on the refractive indices and so also of the chemical composition of the particles. That is out of the scope of the present paper. A comparison of the size distribution, derived from the nephelometer measurements using also the data of the Sevettijärvi filter samples for the calculation of refractive indices, and impactor samples that give the size distribution of the particles in an independent way, will be presented in another paper.

Instead, to retrieve some particle size information of the nephelometer data we now use the same method that Bodhaine (1989) used for the nephelometer measurements at Barrow in 1977–1986. Two values of the Ångström exponent are calculated from the three successive σ_{sp} values according to the formula $\alpha = -\Delta\log(\sigma_{\text{sp}})/\Delta\log(\lambda)$. The interpretation of the Ångström exponent has been discussed, e.g., by Thielke *et al.* (1972) and by Bodhaine and DeLuisi (1985). In general, a large α implies an aerosol size distribution biased

Table 2. Statistics of all measured hourly mean SO_2 concentrations, CN concentrations, particle number concentrations in the accumulation-mode of the mass size distribution ($N_{0.3}$: $0.3 < D_p < 0.5 \mu\text{m}$) and $N_{0.5}$: $D_p > 0.5 \mu\text{m}$), total scattering coefficients (σ_{sp}), backscattering coefficients (σ_{bsp}), backscatter fractions (R), and Ångström exponents (α_{12} and α_{23}). N = number of data points, GM = geometric mean, AM = arithmetic mean, STD = standard deviation.

	N	GM	AM	STD	Percentiles			
					10	50	90	99
SO_2 ($\mu\text{g m}^{-3}$)	27 386	1.05	4.90	18	0.3	0.8	7.7	91
CN (cm^{-3})	19 401	691	1 220	1 697	182	658	2 721	8 817
$N_{0.3}$ (cm^{-3})	11 393	—	—	—	1.9	10.4	33.5	> 35
$N_{0.5}$ (cm^{-3})	11 393	1.3	1.9	3.8	0.36	1.3	4.3	9.7
σ_{sp} (450 nm) (m^{-1})	4 678	1.4×10^{-5}	2.1×10^{-5}	1.9×10^{-5}	4.5×10^{-6}	1.4×10^{-5}	4.8×10^{-5}	8.7×10^{-5}
σ_{sp} (550 nm) (m^{-1})	4 678	1.1×10^{-5}	1.6×10^{-5}	1.5×10^{-5}	3.4×10^{-6}	1.1×10^{-5}	3.6×10^{-5}	7.1×10^{-5}
σ_{sp} (700 nm) (m^{-1})	4 678	7.4×10^{-6}	1.1×10^{-5}	9.8×10^{-6}	2.4×10^{-6}	7.2×10^{-6}	2.3×10^{-5}	4.6×10^{-5}
σ_{bsp} (450 nm) (m^{-1})	4 678	1.6×10^{-6}	2.2×10^{-6}	2.1×10^{-6}	6.5×10^{-7}	1.6×10^{-6}	4.4×10^{-6}	8.2×10^{-6}
σ_{bsp} (550 nm) (m^{-1})	4 678	1.3×10^{-6}	1.7×10^{-6}	1.6×10^{-6}	4.7×10^{-7}	1.2×10^{-6}	3.5×10^{-6}	6.8×10^{-6}
σ_{bsp} (700 nm) (m^{-1})	4 678	1.0×10^{-6}	1.4×10^{-6}	1.3×10^{-6}	3.8×10^{-7}	1.0×10^{-6}	2.8×10^{-6}	5.2×10^{-6}
R (450 nm)	4 678	0.11	0.12	0.04	0.08	0.11	0.16	0.23
R (550 nm)	4 678	0.12	0.12	0.03	0.09	0.12	0.15	0.19
R (700 nm)	4 678	0.14	0.14	0.04	0.11	0.14	0.17	0.23
α_{12}	4 678	1.35	1.80	0.50	0.68	1.61	1.99	2.46
α_{23}	4 678	1.46	1.62	0.59	0.67	1.78	2.22	2.58

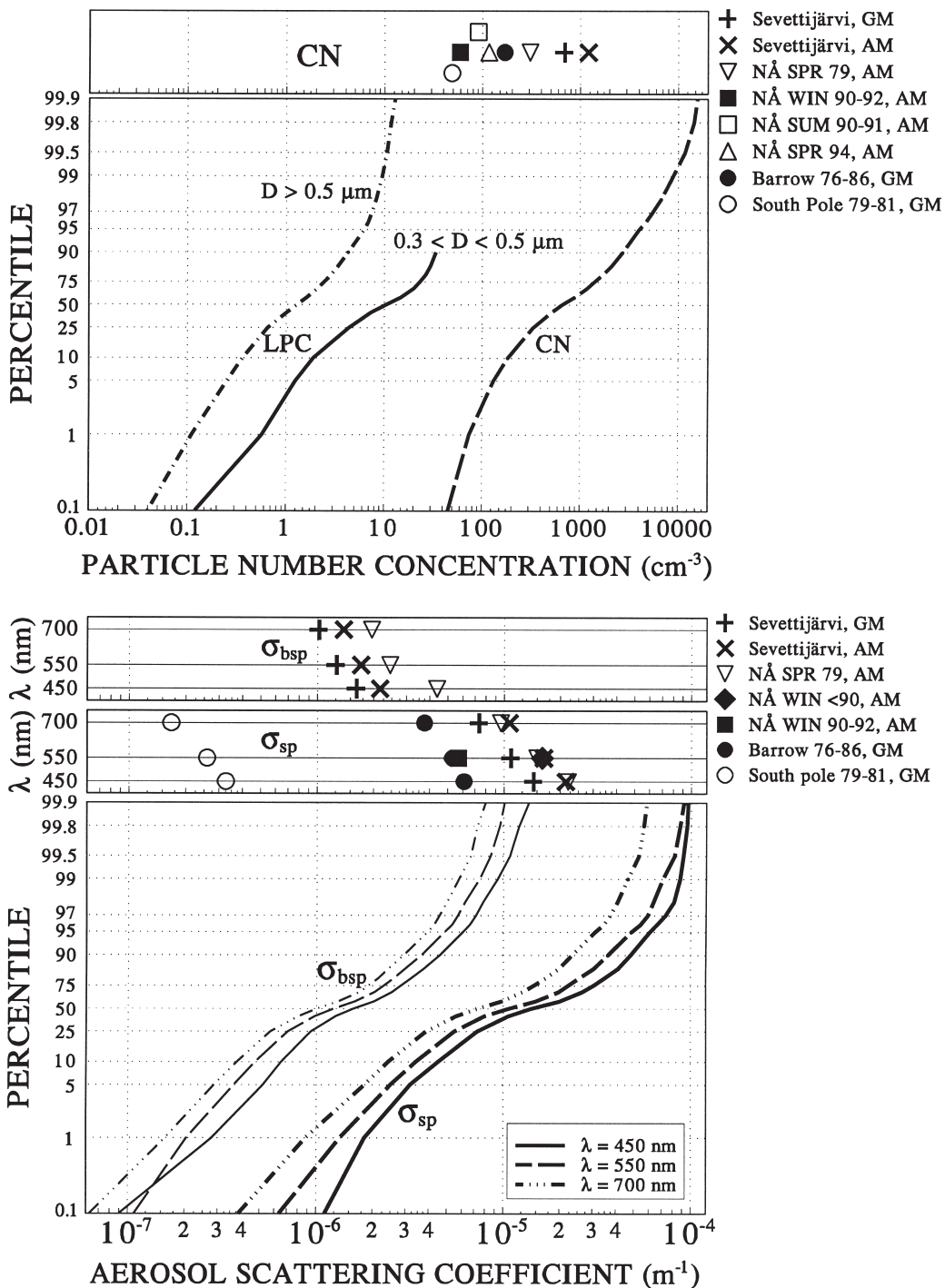


Fig. 4. Cumulative frequency distribution of all hourly mean particle number concentrations and aerosol scattering and backscattering coefficients measured at Sevetijärvi. The upper panel of both charts shows geometric mean (GM) and arithmetic mean (AM) of CN concentrations and scattering coefficients at various locations. The Ny Ålesund (NÅ) means are for spring 1979 (Heintzenberg 1980), for winters 1990–92 and summers 1990–91 (Heintzenberg and Leck 1994), for spring 1994 (Beine *et al.* 1996). The means for Barrow are from Bodhaine (1989), and the means for South Pole from Bodhaine (1983).

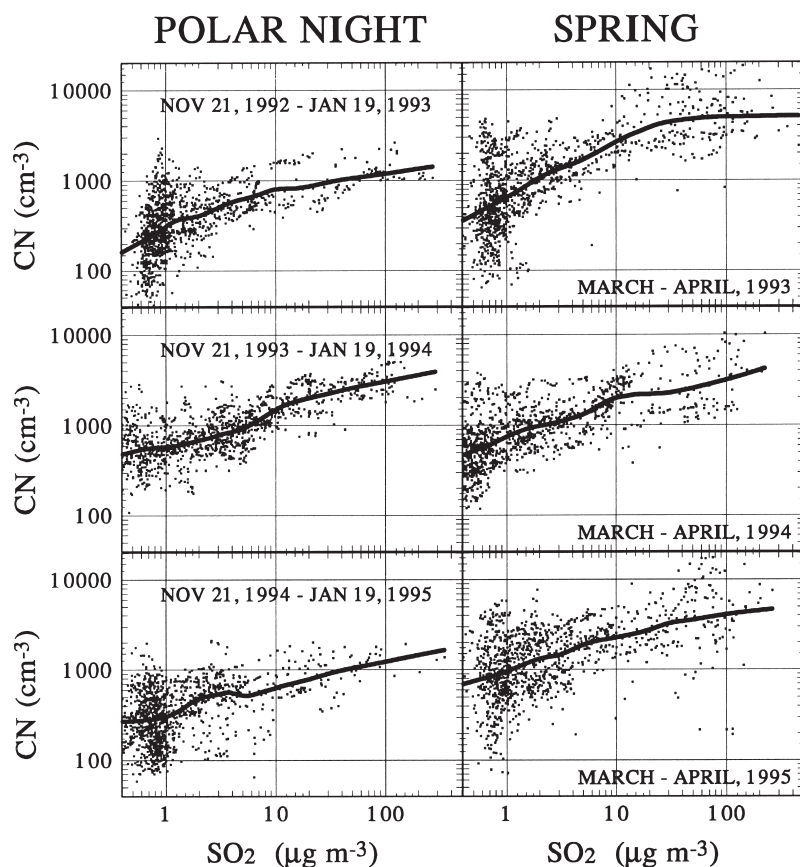


Fig. 5. Relationship between CN concentration and SO_2 concentration during polar night and in spring. The bold lines are locally weighted linear regression of the data points.

toward small particles, and a small α a distribution biased toward large particles. The extinction coefficient and its components are often approximated as being proportional to λ^α (IPCC 1995). Both α and the hemispheric backscattering ratio R ($= \sigma_{\text{bsp}}/\sigma_{\text{sp}}$) are intensive aerosol state parameters that are used in models to calculate the interaction of aerosol particles with solar radiation (IPCC 1995, Ogren 1995). Long time series of α are available from the NOAA baseline stations, e.g., Barrow. Observations in anthropogenically perturbed air masses are available only for a small number of short-duration studies (Ogren 1995). Also, measured values of the hemispheric backscatter ratio R are available only for a small number of short duration studies (Ogren 1995). Heintzenberg (1980) reported 19-day measurements of both σ_{bsp} and σ_{sp} at $\lambda = 450, 550$ and 700 nm at Spitsbergen. From the published average values an estimation for average R and α can be calculated. At the Zeppelin measurement station, Spitsbergen, there is a one-wavelength nephelo-

meter in use (Heintzenberg and Leck 1994) and so it does not give values for R and α .

The geometric mean Ångström exponents α_{12} and α_{23} were 0.70 and 1.53, correspondingly, at Barrow (Bodhaine 1989). At Sevtijärvi the geometric mean α_{12} was 1.35, larger than at Barrow, and the geometric mean α_{23} was 1.46, smaller than at Barrow. This indicates that the aerosol size distribution at these sites is somewhat different. On the other hand, at both sites α is much smaller than the values, practically always > 2 , found during airborne measurements over the United States (Ogren and Sheridan 1996). According to IPCC (1995) the typical ranges of observed backscatter fractions are 0.1–0.2 in polluted continental air and around 0.15 in clean marine air. In their airborne measurements over the United States Ogren and Sheridan (1996) found that the hemispheric backscatter fraction varied in the range 0.11 to 0.18, although it was mostly below 0.13. In the boundary layer they found R to be nearly constant, 0.12. The range of R was larger

at Sevetijärvi (Table 2), but the mean values were close to those mentioned above.

Relationships between the measured quantities

At high SO₂ levels, i.e., during pollution episodes from Nikel, the CN concentrations are practically always high (Fig. 5). At low SO₂ concentrations, on the other hand, the range of CN concentrations is very large. The high CN concentrations at low SO₂ concentrations were usually associated with air masses from Central or Eastern Europe, whereas low CN concentrations and low SO₂ concentrations with air masses from the oceans. The correlation is plotted for both the polar night and spring. As the time series of the monthly geometric mean CN concentrations shows, an increase in CN concentrations is observed when the polar night turns to spring. This rise is also shown by comparing the SO₂–CN data pairs, and it is particularly clear when the polar night of 1992–93 turns to spring 1993, and when the polar night of 1994–95 turns to spring 1995. During the springs of 1993 and 1995, CN concentrations higher than 10 000 cm⁻³ are frequently detected in plumes from Nikel.

According to Kerminen and Wexler (1996), binary homogeneous nucleation between water and sulphuric acid is favoured by a high SO₂ to fine particle mass ratio, of the order of one or greater. In the Nikel plumes, the SO₂ concentration varies between 100 and 500 µg m⁻³. Waggoner and Weiss (1980) found a linear relationship between light scattering at 550 nm and total aerosol mass, $m(\text{g m}^{-3}) = 0.32\sigma_{\text{sp}}$. The highest measured scattering coefficients at Sevetijärvi are $< 10^{-4} \text{ m}^{-1}$, so the mass concentrations can be estimated to be $< 32 \text{ µg m}^{-3}$. Thus, the SO₂ to particle mass ratio in the plumes is much larger than one. Nucleation is also favoured by cool and humid ambient conditions, and by strong solar radiation (Kerminen and Wexler 1995). Relative humidity is often high during the episodes, because the plumes from Nikel are often mixed with humid air from the Barents Sea. Especially in spring and in autumn, all the required conditions for nucleation are fulfilled during the Nikel pollution episodes at Sevetijärvi.

Fig. 5 also shows that the highest particle number

concentrations did not occur concurrently with the highest SO₂ concentrations ($> 200 \text{ µg m}^{-3}$), but with concentrations around 100 µg m^{-3} . This may be due to the short transport times ($< 6 \text{ h}$) from the smelters during the strongest SO₂ episodes. In these cases, the airborne sulphate particles have probably not had a sufficient time to grow to a size at which they can be detected by the CPC, i.e., their diameter was less than 14 nm.

Fig. 6 shows that generally the scattering coefficients were high and the backscatter fractions were low in pollution plumes, i.e., when SO₂ concentration was high. It also shows that in pollution plumes α was generally higher, so that the size distribution is biased towards small particles more in the polluted air than in the air with low SO₂ concentrations. In air with low SO₂ concentrations the range of all these properties is large indicating various source areas. The backscatter fraction R shows a clear inverse relationship with σ_{sp} (Fig. 7). This effect is greater at lower wavelengths. The range of R in air with low SO₂ concentrations is much larger than in air with low σ_{sp} , which shows that low σ_{sp} is a better indicator of clean air than low SO₂ concentration. The geometric mean backscatter fraction was slightly higher in summer than in winter (Fig. 3). The inverse relationship between R and σ_{sp} shows that this is due to lower scattering coefficients measured during May and June.

Source analyses

Wind statistics

Wind measurements were grouped into eight sectors. The centres of the sectors are: 0° (N), 45° (NE), 90° (E), 135° (SE), 180° (S), 225° (SW), 270° (W), and 315° (NW). The direction of Nikel is 105° from the station, which means that winds blowing directly from Nikel to Sevetijärvi are classified in sector E. All measured quantities were classified according to wind direction. In Fig. 8 the arithmetic means of some of them in the various wind sectors are illustrated using wind roses. The wind distribution according to its direction and speed is also presented. The prevailing winds at the station are from the SW, comprising approximately 30% of observations.

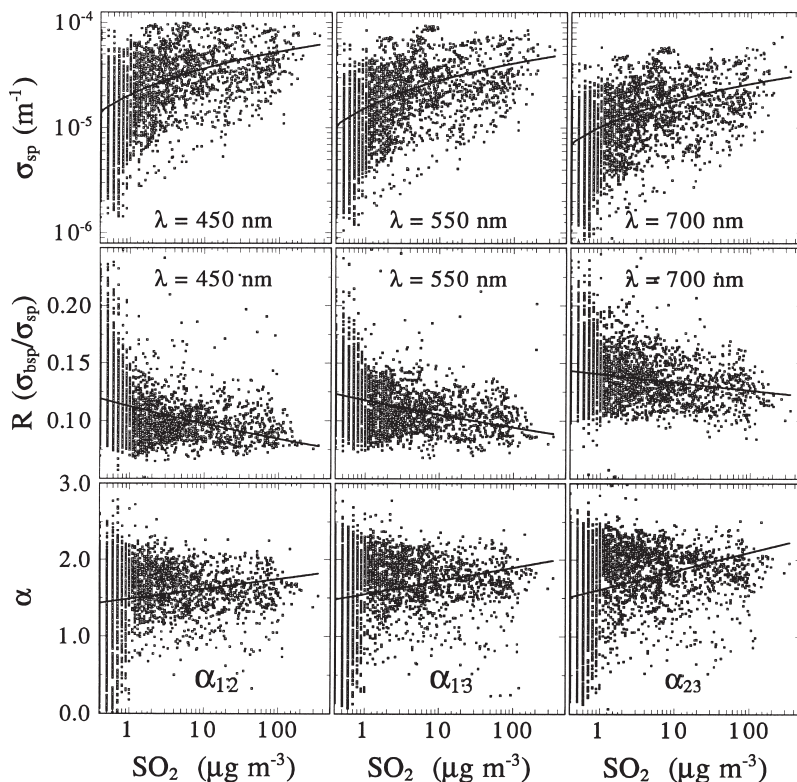


Fig. 6. Relationships between SO_2 and σ_{sp} , SO_2 and the backscatter fraction R , and SO_2 and α . The lines are fitted logarithmic (for SO_2 - σ and SO_2 - α) and power curves (for SO_2 - R).

The SO_2 and particle number concentrations were highest in the direction of Nikel, sector E, as was the case for mean scattering coefficients also, but not as clearly. The lowest mean SO_2 and particle number concentrations, and lowest mean scattering coefficients and the highest hemispheric backscatter fractions were detected during winds from the NW sector, the direction to the Norwegian Sea. There were more frequently winds from the W and NW sectors during May and June 1995 than in the preceding winter. This explains the lower scattering coefficients and also the higher backscatter fractions measured in May and June 1995 than in winter (Fig. 3).

As discussed previously, a large Ångström exponent α implies a particle size distribution biased toward small particles, and a small α towards large particles. The wind rose of α_{12} shows that aerosols from the sectors NW, N, and NE have size distributions biased more towards large particles than aerosol from southern sectors. This is credible, since air from these sectors has a marine signature with large sea-salt particles from the

Norwegian and Barents Seas.

The sectors E, S, and NW were selected to represent the air from Nikel, from the continental Europe, and from the Arctic Ocean, respectively. The mean values of SO_2 and some selected aerosol properties together with their cumulative distributions, as measured during winds from sectors E, S and NW, are presented in Table 3. For the particle properties in Table 3, additional conditions have been used: sector E: $[\text{SO}_2] > 20 \mu\text{g m}^{-3}$, in order to take into account only the concentrations in the pollution plumes from Nikel; sector S: $[\text{SO}_2] < 25 \mu\text{g m}^{-3}$, in order to eliminate at least the most evident Nikel pollution plumes and thus classify the southern winds more or less to continental air excluding the Kola area; and finally sector NW: $[\text{SO}_2] < 1 \mu\text{g m}^{-3}$, in order to eliminate clear pollution episodes both from Nikel and other sources and thus classify the sector to marine air. The data for SO_2 , CN, LPC, and σ_{sp} cover different time periods, but the distribution of the wind in different sectors during all these periods was almost the same. The percentage of

Fig. 7. Relationship between the hemispheric backscatter fraction and σ_{sp} . The lines are fitted power curves: $R(450\text{nm}) = 0.012 \times \sigma_{sp}^{-0.20}$, $R(550\text{nm}) = 0.021 \sigma_{sp}^{-0.15}$, $R(700\text{ nm}) = 0.038 \sigma_{sp}^{-0.11}$, the symbols are geometric mean values from each wind sector (with the SO_2 conditions of Table 3), and the error bars the 10th and the 90th percentiles.

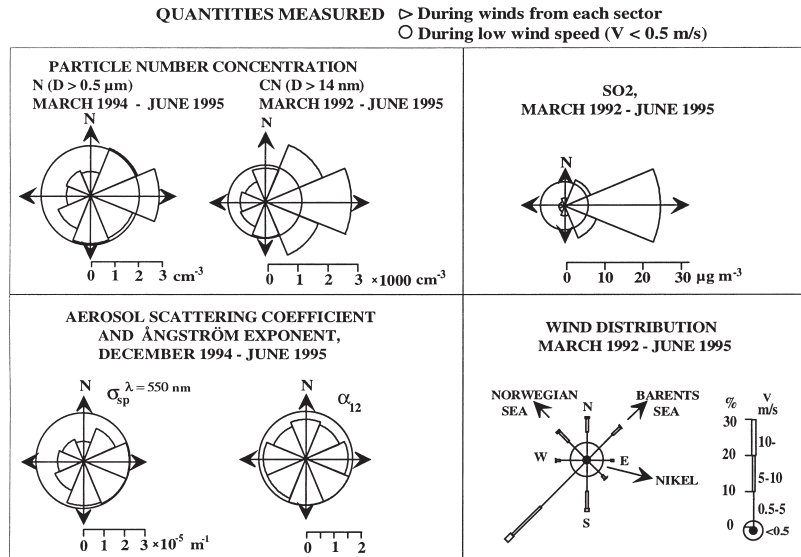
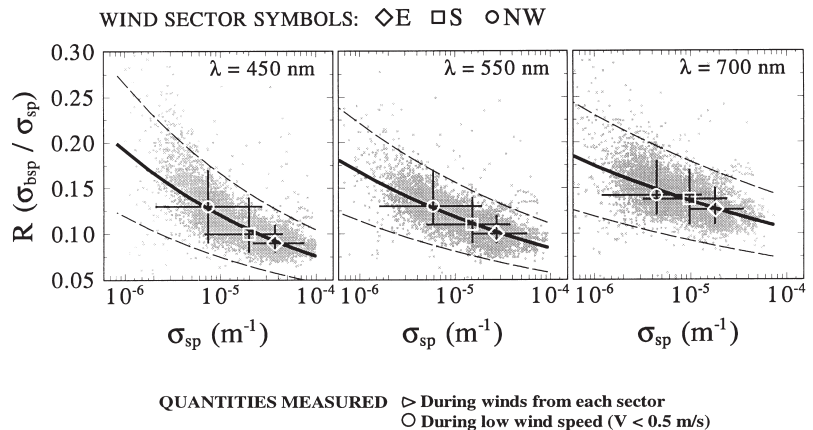


Fig. 8. Arithmetic mean particle number concentrations, sulphur dioxide concentrations, aerosol scattering coefficients and Ångström exponents measured during wind from different sectors, and wind distribution at Sevetijärvi between 1992 and 1995.

winds from sectors E, S, and NW was approximately 6%, 12%, and 9%, respectively.

Trajectory analyses

An episode with long-range transport of pollution

The measurements on December 19–23, 1994, provide a good example of long-range transport of aerosols and of differences between continental and marine air. The measured quantities are plotted in Fig. 9. The 96-h back-trajectories arriving at the 950 hPa pressure level, at noon each day, are also shown. There is a clear decrease in all quantities as the origin of the air changes from eastern Europe to the Northern Atlantic or the Arctic Ocean. In this exam-

ple, the SO_2 concentration rises to approximately $2.5 \mu\text{g m}^{-3}$ in air masses which have traversed continental Europe. This is typical in Lapland during pollution episodes from eastern Europe, but occasionally, in winter, the SO_2 concentration may exceed $20 \mu\text{g m}^{-3}$ in these episodes.

An analysis of synoptic weather charts shows that between December 17 and 20, 1994, a cyclone positioned initially over Iceland moved eastwards. At the same time an anticyclone was situated over eastern Europe, and northward transport of pollution between the cyclone and anticyclone was established. Raatz (1991) has shown that this is a typical transport pathway for pollutants to the Norwegian Arctic. On December 21 the centre of the cyclone had moved to the Barents Sea, and an anticyclone was situated over the British Isles. During the following days a high pres-

sure area covered the whole of Europe, resulting in a westerly flow over the Norwegian Sea, and in transport of marine air to the measurement site.

Trajectory statistics

As a large set of trajectories and measurement data was available, the statistical method developed by Stohl (1996) was used to identify source areas. The method utilises ambient air pollutant concentration measurements at a receptor site, and the

corresponding back-trajectories arriving at that site. The Sevettijärvi virtual impactor samples have been previously analysed using this method to find the source areas of sulphate, ammonium, and sodium (Virkkula *et al.* 1995). The procedure calculates the geometric mean concentration that is observed at the receptor site when trajectories have crossed each cell of a geographical grid which is superimposed on the domain of the trajectory computations. The geometric mean is weighted by the residence time of the trajectory in each grid cell according to the formula:

Table 3. Statistics of hourly mean SO₂ concentrations, particle number concentrations (CN and N_{0.5}), scattering coefficients (σ_{sp} and σ_{bsp}), R and Ångström exponents (α), during winds from three sectors: E (90°), S (180°), and NW (315°). For particle properties, additional conditions has been used: E: [SO₂] > 20 μg m⁻³, S: [SO₂] < 25 μg m⁻³, NW: [SO₂] < 1 μg m⁻³.

	Sector Center	N	GM	AM	STD	Percentiles			
						10	50	90	99
SO ₂ (μg m ⁻³)	E	1 467	5.5	25	45	0.5	5.3	81	210
	S	3 100	1.4	3.1	10.3	0.4	1.2	6.2	26
	NW	2 330	0.6	1.6	7.5	< 0.3	0.6	1.4	22
CN (cm ⁻³)	E	398	3 310	4 540	3 790	1 260	3 090	10 300	16 200
	S	2 306	831	1 120	965	324	779	2 320	4 680
	NW	1 188	331	584	918	103	297	1 280	5 500
N _{0.5} (cm ⁻³)	E	207	4	4.6	2.4	2.1	3.7	8.6	11.2
	S	1 163	1.8	2.5	2.1	0.5	1.7	5.6	10.4
	NW	696	0.7	1.1	0.9	0.2	0.9	2.2	4.7
σ _{sp} (m ⁻¹) (450 nm)	E	101	3.7 × 10 ⁻⁵	4.1 × 10 ⁻⁵	1.9 × 10 ⁻⁵	2.2 × 10 ⁻⁵	3.5 × 10 ⁻⁵	7.5 × 10 ⁻⁵	8.9 × 10 ⁻⁵
	S	606	2.0 × 10 ⁻⁵	2.6 × 10 ⁻⁵	1.8 × 10 ⁻⁵	6.8 × 10 ⁻⁶	2.2 × 10 ⁻⁵	4.5 × 10 ⁻⁵	9.1 × 10 ⁻⁵
	NW	251	7.4 × 10 ⁻⁶	1.1 × 10 ⁻⁵	9.8 × 10 ⁻⁶	2.1 × 10 ⁻⁶	7.7 × 10 ⁻⁶	2.7 × 10 ⁻⁵	4.4 × 10 ⁻⁵
σ _{sp} (m ⁻¹) (550 nm)	E	101	2.7 × 10 ⁻⁵	3.0 × 10 ⁻⁵	1.5 × 10 ⁻⁵	1.6 × 10 ⁻⁵	2.6 × 10 ⁻⁵	5.7 × 10 ⁻⁵	6.8 × 10 ⁻⁵
	S	606	1.5 × 10 ⁻⁵	2.1 × 10 ⁻⁵	1.8 × 10 ⁻⁵	5.0 × 10 ⁻⁶	1.7 × 10 ⁻⁵	3.8 × 10 ⁻⁵	8.8 × 10 ⁻⁵
	NW	251	5.9 × 10 ⁻⁶	8.2 × 10 ⁻⁶	7.0 × 10 ⁻⁶	1.6 × 10 ⁻⁶	6.5 × 10 ⁻⁶	1.9 × 10 ⁻⁵	3.3 × 10 ⁻⁵
σ _{sp} (m ⁻¹) (700 nm)	E	101	1.8 × 10 ⁻⁵	2.0 × 10 ⁻⁵	1.1 × 10 ⁻⁵	1.0 × 10 ⁻⁵	1.7 × 10 ⁻⁵	3.6 × 10 ⁻⁵	4.4 × 10 ⁻⁵
	S	606	9.7 × 10 ⁻⁶	1.3 × 10 ⁻⁵	1.1 × 10 ⁻⁵	3.3 × 10 ⁻⁶	1.1 × 10 ⁻⁵	2.4 × 10 ⁻⁵	5.5 × 10 ⁻⁵
	NW	251	4.4 × 10 ⁻⁶	6.0 × 10 ⁻⁶	4.6 × 10 ⁻⁶	1.2 × 10 ⁻⁶	5.2 × 10 ⁻⁶	1.3 × 10 ⁻⁵	2.3 × 10 ⁻⁵
σ _{bsp} (m ⁻¹) (450 nm)	E	101	3.4 × 10 ⁻⁶	3.7 × 10 ⁻⁶	1.6 × 10 ⁻⁶	2.0 × 10 ⁻⁶	3.2 × 10 ⁻⁶	6.5 × 10 ⁻⁶	8.4 × 10 ⁻⁶
	S	606	2.0 × 10 ⁻⁶	2.4 × 10 ⁻⁶	1.7 × 10 ⁻⁶	8.4 × 10 ⁻⁷	2.1 × 10 ⁻⁶	3.9 × 10 ⁻⁶	9.9 × 10 ⁻⁶
	NW	251	9.5 × 10 ⁻⁷	1.2 × 10 ⁻⁶	8.6 × 10 ⁻⁷	3.6 × 10 ⁻⁷	1.0 × 10 ⁻⁶	2.5 × 10 ⁻⁶	4.0 × 10 ⁻⁶
σ _{bsp} (m ⁻¹) (550 nm)	E	101	2.8 × 10 ⁻⁶	3.0 × 10 ⁻⁶	1.3 × 10 ⁻⁶	1.6 × 10 ⁻⁶	2.7 × 10 ⁻⁶	5.4 × 10 ⁻⁶	6.6 × 10 ⁻⁶
	S	606	1.5 × 10 ⁻⁶	1.9 × 10 ⁻⁶	1.4 × 10 ⁻⁶	6.2 × 10 ⁻⁷	1.7 × 10 ⁻⁶	3.1 × 10 ⁻⁶	7.6 × 10 ⁻⁶
	NW	251	7.7 × 10 ⁻⁷	9.9 × 10 ⁻⁷	7.1 × 10 ⁻⁷	2.7 × 10 ⁻⁷	8.5 × 10 ⁻⁷	2.0 × 10 ⁻⁶	3.3 × 10 ⁻⁶
σ _{bsp} (m ⁻¹) (700 nm)	E	101	2.3 × 10 ⁻⁶	2.5 × 10 ⁻⁶	1.0 × 10 ⁻⁶	1.3 × 10 ⁻⁶	2.2 × 10 ⁻⁶	4.4 × 10 ⁻⁶	4.9 × 10 ⁻⁶
	S	606	1.2 × 10 ⁻⁶	1.5 × 10 ⁻⁶	1.1 × 10 ⁻⁶	4.8 × 10 ⁻⁷	1.3 × 10 ⁻⁶	2.5 × 10 ⁻⁶	5.5 × 10 ⁻⁶
	NW	251	6.3 × 10 ⁻⁷	8.2 × 10 ⁻⁷	5.8 × 10 ⁻⁷	2.0 × 10 ⁻⁷	7.2 × 10 ⁻⁷	1.6 × 10 ⁻⁶	2.8 × 10 ⁻⁶
R (450 nm)	E	101	0.09	0.09	0.01	0.08	0.09	0.11	0.13
	S	606	0.10	0.10	0.02	0.08	0.10	0.14	0.19
	NW	251	0.13	0.13	0.04	0.09	0.13	0.17	0.29
R (550 nm)	E	101	0.10	0.10	0.01	0.09	0.10	0.12	0.13
	S	606	0.11	0.11	0.02	0.09	0.11	0.14	0.16
	NW	251	0.13	0.13	0.03	0.11	0.13	0.17	0.24
R (700 nm)	E	101	0.13	0.13	0.01	0.11	0.13	0.15	0.17
	S	606	0.14	0.14	0.02	0.11	0.14	0.17	0.20
	NW	251	0.14	0.15	0.04	0.12	0.14	0.18	0.29
α ₁₂	E	101	1.51	1.56	0.32	1.37	1.61	1.84	2.02
	S	606	1.60	1.65	0.32	1.27	1.69	1.95	2.30
	NW	251	0.86	1.17	0.67	0.24	1.20	2.00	2.56
α ₂₃	E	102	1.73	1.78	0.34	1.45	1.81	2.10	2.28
	S	606	1.82	1.87	0.38	1.32	1.96	2.21	2.48
	NW	251	0.92	1.17	0.70	0.28	1.11	2.14	2.65

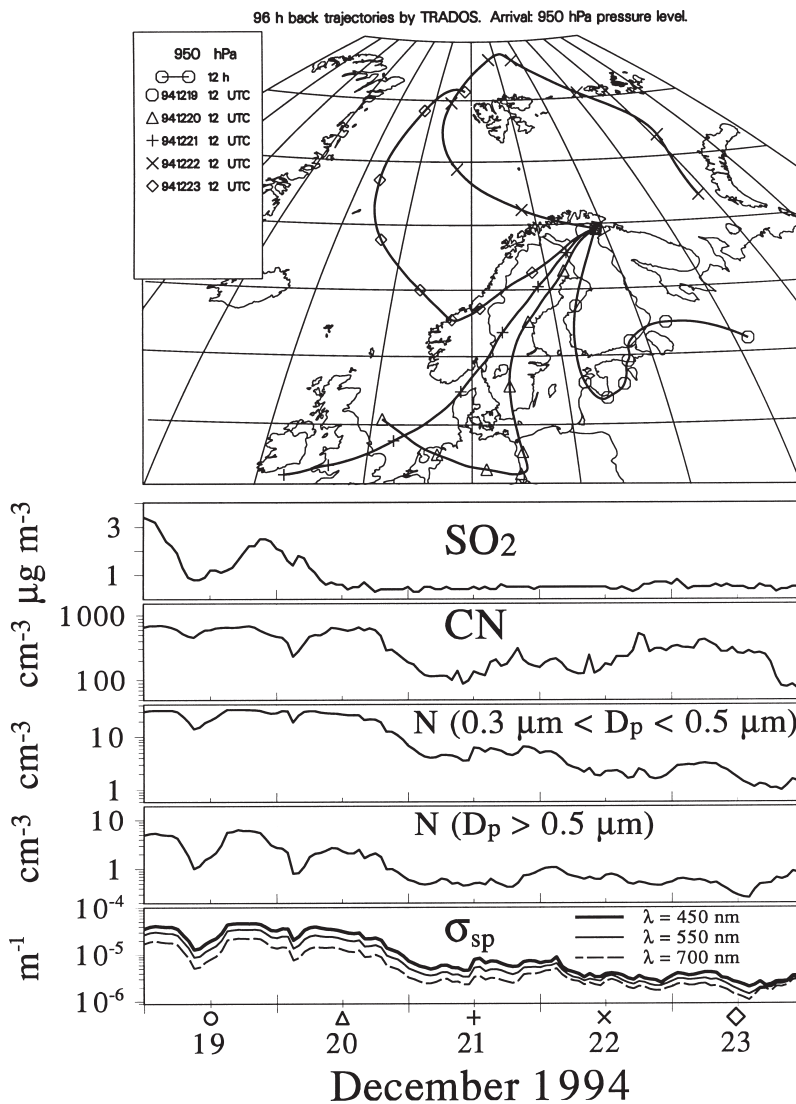


Fig. 9. An example of long-range transport of sulphur dioxide and aerosols. The identifying symbols of the trajectories are plotted on the time axis to denote the arrival times of each trajectory. The symbols on the trajectories show the distance travelled during 12 hours.

$$\log(\text{GMC}_{mn}) = \frac{\sum_l \log(C_l) \tau_{mnl}}{\sum_l \tau_{mnl}} \quad (2)$$

where GMC_{mn} is the geometric mean concentration, m and n are the indices of the horizontal grid, l is the index of the trajectory, C_l is the concentration observed on the arrival of trajectory l and τ_{mnl} is the time spent in grid element (m,n) by the trajectory l . $\log(\text{GMC}_{mn})$ serves as a first-guess field that is treated by an iterative redistribution that improves the spatial resolution of the first-guess field, and that reveals more detailed fine-scale structures. The method also includes a smoothing

procedure (Seibert *et al.* 1994), where a confidence interval is calculated for each grid cell and the field is repeatedly smoothed with a 9-point filter, imposing the restriction that the values must be kept within their confidence intervals. This procedure removes insignificant features but preserves the significant ones. For a more detailed description of the method see Stohl (1996).

The value for a grid cell is calculated only if a minimum number of trajectories crosses it. The time series of SO_2 and particle number concentrations are so long that a minimum of 20 trajectories in a grid square was set. The scattering coefficient time series is only eight months in length, and thus a minimum number of 15 was used.

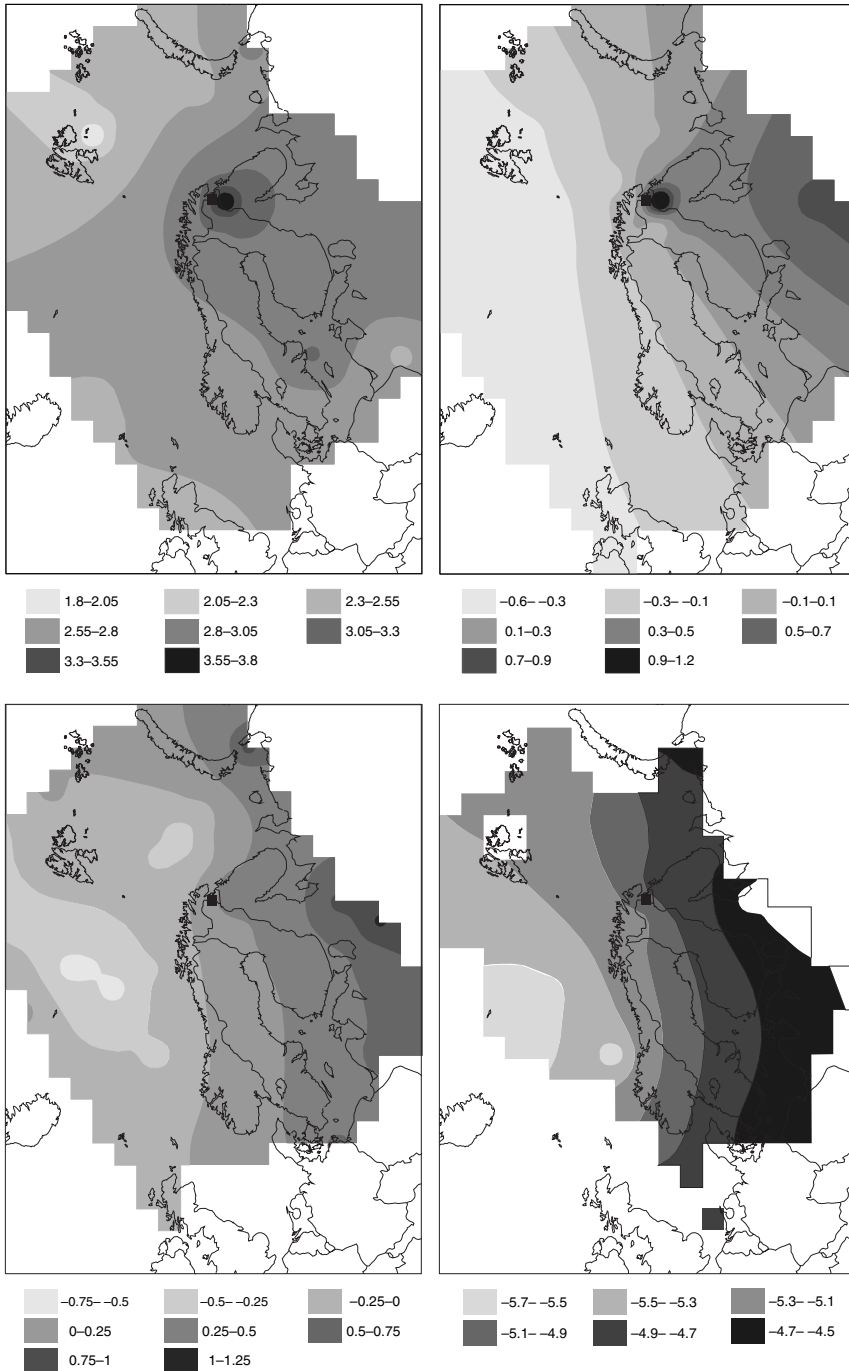


Fig. 10. The geometric mean sulphur dioxide concentration, particle number concentration and aerosol scattering coefficient at Sevetijärvi, when the trajectories have passed over each grid square. The 3-dimensional trajectories used for the analysis arrive at the 950 hPa level. The concentrations are expressed in $lg(C)$, where C is the concentration. For SO_2 , CN , and LPC , the white areas are those grid squares, which have been crossed by less than 20 trajectories, but for σ_{sp} those grid squares, which have been crossed by less than 15 trajectories. Top left: $lg[CN \text{ (cm}^{-3}\text{)}]$, top right: $lg[SO_2 \text{ (}\mu\text{g m}^{-3}\text{)}]$, bottom left: $lg[N(D > 0.5 \mu\text{m}, \text{cm}^{-3})]$, bottom right subfigure: $lg[\sigma_{sp} \text{ (550 nm, m}^{-1}\text{)}]$.

It was previously stated that three or four back-trajectories for each day were calculated. In other words, the interval between the arrivals is 6 or 8 hours. The pollution episodes from Nickel frequently only last a few hours, so it is possible that an episode occurring between the arrival of two successive trajectories would not be included in the determination of the source area. Because of this problem, 8-hour running means of all measured quantities were calculated before applying the trajectory statistics.

The 3D-trajectories arriving at the 950-hPa level, approximately 500 m asl, were used in the statistics. Boundary layer heights are usually shallow in the Arctic, because of lack of solar heating and upward sensible heat flux. Therefore we chose a rather low arrival height of the trajectories. Another reason is that the distance to Nickel is only 60 km and the higher trajectories often fail to show this short-range transport because of a decoupling between the free troposphere and the boundary layer. Also Beine *et al.* (1996) used trajectories arriving at 950 hPa to examine the source areas of aerosol in Spitsbergen. Trajectories arriving at the surface level and at the 900-hPa level were also calculated. Using them in the statistics leads to somewhat different locations of the isolines, but the basic picture — a sharp contrast between marine and continental air — remains.

The results are presented in Fig. 10. For SO₂, the statistics show Nickel as the dominant source area. It also shows that concentrations are higher during flows from the continental Europe than during flows from the ocean. The range of geometric mean SO₂ concentrations for air which has passed over Nickel is from 10^{0.7} to 10^{1.2} μg m⁻³, i.e., from 5 to 16 μg m⁻³. This is consistent with the geometric mean concentration in the wind sector E, which is 5.5 μg m⁻³ (Table 3). The position of the highest SO₂ source area is somewhat south of Nickel, but becomes closer to the real position of Nickel if trajectories arriving at the surface are used. However, surface trajectories are not so representative for studying long-range transport.

The major source area for CN is Nickel, and lower concentrations are observed in air masses arriving from the rest of the continent. In the case of marine air measured at Sevetijärvi, CN concentrations in air which has traversed the Norwe-

gian Sea are much higher than those in air coming from the Arctic Sea. This can be interpreted so that the Norwegian Sea is a source for freshly-nucleated particles.

According to the analysis, high particle number concentrations in the accumulation-mode of the mass size distribution were brought to Finnish Lapland from the whole continental Europe. Nickel does not show out as clearly as a source area neither for the particle number concentrations at the $D > 0.5$ μm size range, nor for high σ_{sp} , as it does for SO₂ and CN. The wind roses of $N(D_p > 0.5 \mu\text{m})$ and σ_{sp} (Fig. 8), on the other hand, did show the highest mean concentrations in the sector pointing towards Nickel. This discrepancy can be due to various reasons: it may be that the time series of LPC and nephelometer measurements are not quite long enough for the trajectory statistical analysis. But it can also be due to both the concentration range intervals and the smoothing parameters chosen for the trajectory statistics. On the other hand, the highest episodic peaks of σ_{sp} (550 nm), close to 10⁻⁴ m⁻¹, were measured in air masses which were calculated to have passed over Eastern Europe, Poland. These scattering coefficients are those high σ_{sp} points in Fig. 6 where SO₂ concentrations are between 5–10 μg m⁻³.

All the source analyses give high concentrations when air comes from south-east of Novaja Zemlja. Two major sources of Arctic air pollution are the Pechora basin, located south of Novaja Zemlja, and the Norilsk area, located south-east of Novaja Zemlja (Ottar 1989). Thus, the trajectory statistical analyses suggest that the impact of these Siberian sources can be detected at Sevetijärvi, despite the vicinity of the very large source at Nickel only 60 km east-southeast of the station.

Values obtained from Fig. 10 are shown in Table 4, which gives the ranges of geometric mean concentrations at Sevetijärvi when the source area is either the Kola peninsula (class A), continental Europe (class B), the Norwegian Sea (class C), or the Arctic Sea (class D). The values of Table 4 are compared in Fig. 11 to the geometric means of the quantities measured during winds from the corresponding sectors. In Fig. 11 the wind classification is shown twice: using all data that is measured during winds from the corresponding sector and using only data that is classified both by wind sectors and by the SO₂ concentration conditions

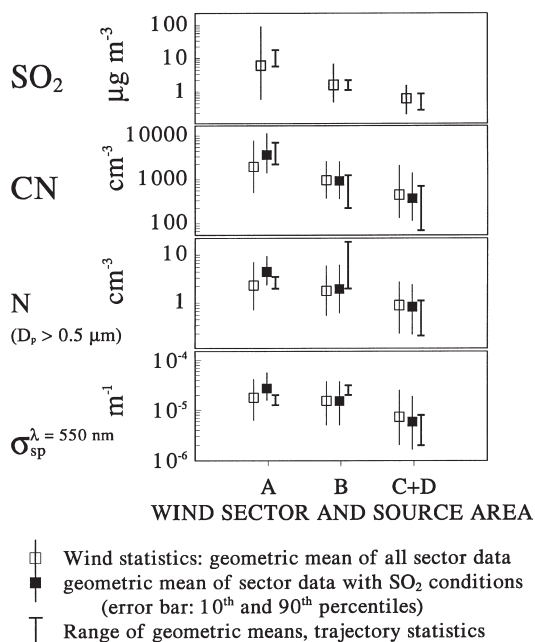


Fig. 11. Comparison of wind and trajectory statistics. The wind sectors are: A: from 67.5° to 112.5° (centre 90°, east), B: from 157.5° to 202.5° (centre 180°, south), and C+D: from 292.5° to 337.5° (centre 315°, north-west). The corresponding source areas of the trajectory statistics are: A: the Kola Peninsula, B: Continental Europe, and C + D: the Norwegian Sea and the Arctic Sea.

that were used for Table 3.

For SO_2 , the geometric means of the wind sectors fall within the ranges given by the trajectory statistics in all categories, even though the trajectory statistics suggest somewhat larger differences between different source areas compared with the wind statistics. For CN, too, both methods give qualitatively the same results, although the ranges of both wind and trajectory statistics are large. For accumulation-mode particles and scattering coefficients, the results are similar, as far as categories A and C+D are concerned. The obvious

difference is that the trajectory statistics give higher values in the continental Europe — southern wind category (B).

Summary and conclusions

The aim of this work was to find how much the closely-located large pollution sources in the Kola peninsula influence the aerosol measurements at Sevettijärvi. The mean and variability of particle concentrations at the site are higher than at cleaner sites like Barrow, Alaska, and Ny Ålesund, Spitsbergen. Nevertheless, the trajectory statistical analysis shows that the lowest CN concentrations, detected in air masses traversed over the Arctic Sea (Table 4), are comparable with the concentrations at Spitsbergen and Barrow. When air masses originate from over the Norwegian Sea the CN concentrations are higher than in air traversed over the Arctic Sea. For larger particles — i.e., particles of the size of the accumulation mode of the mass size distribution — the situation is the opposite. These are similar observations to those of Beine *et al.* (1996). They found at Spitsbergen that in the background air, during flows from the Arctic Sea or the Norwegian Sea, the median $\sigma_{\text{sp}}(550 \text{ nm})$ was 3.8×10^{-6} and $1.3 \times 10^{-6} \text{ m}^{-1}$, respectively, and CN concentrations of 180 and 270 cm^{-3} , respectively. The values in Table 4 are not only qualitatively but also quantitatively similar. The most likely reason for the difference in the aerosol concentrations in the air masses flow from over the Norwegian and Arctic Seas is the difference in natural sulphur emissions and resulting secondary particle production between these two areas. Open high-latitude oceans are strong DMS emitters, while the ocean north of Spitsbergen is usually frozen (Heintzenberg and Leck 1994). Thus, by measuring CN at one point,

Table 4. Ranges of geometric means according to trajectory statistics. A: the Kola peninsula, B: Continental Europe, C: the Norwegian Sea, and D: the Arctic Sea.

	Source area			
	A	B	C	D
$\text{SO}_2 (\mu\text{g m}^{-3})$	5.0–15.9	0.5–3.2	0.25–0.5	0.25–0.8
$\text{CN} (\text{cm}^{-3})$	1 995–6 310	200–1 122	112–354	63–199
$N_{0.5} (\text{cm}^{-3})$	1.8–3.2	1.8–17.8	0.2–1	1–1.8
$\sigma_{\text{sp}}(550) (\text{m}^{-1})$	1.3×10^{-5} – 2.0×10^{-5}	2.0×10^{-5} – 3.2×10^{-5}	2.0×10^{-6} – 5.0×10^{-6}	5.0×10^{-6} – 7.9×10^{-6}

Sevettijärvi, and combining the data with back-trajectories, we have been able to approximately determine where the ice cover in the Arctic Sea starts.

The Kola peninsula pollution sources do not totally screen the more eastern source areas in northern Siberia. The observation that these pollution sources can be seen in the trajectory statistical images, further shows that the trajectory statistics is a powerful method. It also shows that the back-trajectories used for the calculations were generally accurate, although it gives no indication of the errors in individual trajectories.

One of the aims of this paper was to find classification criteria for all subsequent analyses of Sevettijärvi aerosol and gas measurements. None of the suggested criteria alone — particle number concentrations, light scattering coefficients, sulphur dioxide concentrations, wind direction and modelled air mass trajectories — provides an unambiguous criterion. To classify air into air masses from the Arctic Sea and the Norwegian Sea or from Continental Europe trajectories work best. Generally, also the trajectories are good indicators for the Kola peninsula pollution episodes, as the trajectory statistics of SO₂ and CN showed. Nevertheless, trajectories failed to present some of the pollution episodes from the Kola peninsula. The best indicator of these is high SO₂ concentration. On the other hand, it was shown that low σ_{sp} is a better indicator of clean air than low SO₂ concentration. The comparison between the wind and trajectory statistics showed that at Sevettijärvi, by using surface-wind measurements only, the air masses can roughly be classified into three categories: during easterly winds air arrives predominantly from the Kola peninsula, during southerly winds from continental Europe, and during northwesterly winds from the Norwegian Sea.

Acknowledgement: This study was funded partly by the Lapland Forest Damage Project.

References

- Anderson T.L., Covert D.S., Marshall S.F., Laucks M.L., Charlson R.J., Waggoner A.P., Ogren J.A., Caldwell R., Holm R.L., Quant F.R., Sem G.J., Wiedensohler A., Ahlquist N.A. & Bates T.S. 1996. Performance characteristics of a high-sensitivity, three-wavelength, total scatter/backscatter nephelometer. *J. Atmos. Oceanic Technol.* 13: 967–986.
- Barrie L.A., den Hartog G., Bottenheim J.W. & Landsberger S. 1989. Anthropogenic aerosols and gases in the lower troposphere at Alert Canada in April 1989. *J. Atmos. Chem.* 9: 101–127.
- Beine H.J., Engardt M., Jaffe D.A., Hov Ø, Holmén K. & Stordal F. 1996. Measurements of NO_x and aerosol particles at the Ny Ålesund Zeppelin mountain station on Svalbard: influence of regional and local pollution sources. *Atmos. Environ.* 30: 1067–1079.
- Bodhaine B.A. 1983. Aerosol measurements at four background sites. *J. Geophys. Res.* 88: 10753–10768.
- Bodhaine B.A. & DeLuisi J.J. 1985. An aerosol climatology of Samoa. *J. Atmos. Chem.* 3: 107–122.
- Bodhaine B.A. 1989. Barrow surface aerosol: 1976–1986. *Atmos. Environ.* 23: 2357–2369.
- Bodhaine B.A., Ahlquist N.C. & Schnell R.C. 1991. Three-wavelength nephelometer suitable for aircraft measurement of background aerosol scattering coefficient. *Atmos. Environ.* 25A: 2267–2276.
- Brockman J.E. 1993. Sampling and Transport of Aerosols. In Willeke K. & Baron P (ed.) *Aerosol measurement: principles, techniques, and applications* Van Nostrand Reinhold, New York, 1993. pp. 77–111.
- Covert D.S. & Heintzenberg J. 1993. Size distributions and chemical properties of aerosol at Ny Ålesund, Svalbard. *Atmos. Environ.* 27A: 2989–2998.
- Djupström M., Pacyna J.M., Maenhaut W., Winchester J.W., Li S.-M. & Shaw G.E. 1993. Contamination of Arctic air at three sites during a haze event in late winter 1986. *Atmos. Environ.* 27A: 2999–3010.
- Djupström-Fridell M. 1995. Trace elements in airborne particles as observed at remote locations. PhD Thesis, Department of Physics, Chalmers University of Technology, Göteborg, Sweden.
- Heidam N.Z., Wählin P. & Kemp K. 1993. Arctic aerosols in Greenland. *Atmos. Environ.* 27A: 3029–3036.
- Heintzenberg J. 1980. Particle size distribution and optical properties of Arctic haze. *Tellus* 32: 251–260.
- Heintzenberg J., Hansson H.-C. & Lannefors H. 1981. The chemical composition of arctic haze at Ny-Aalesund, Spitsbergen. *Tellus* 33: 162–171.
- Heintzenberg J., Stroem, J., Ogren, J.A. & Fimpel H.-P. 1991. Vertical profiles of aerosol properties in the summer troposphere of the European Arctic. *Atmos. Environ.* 25A: 621–628.
- Heintzenberg J. & Leck C. 1994. Seasonal variation of the atmospheric aerosol near the top of the marine boundary layer over Spitsbergen related to the Arctic sulphur cycle. *Tellus* 46B: 52–67.
- Hillamo R.E., Kerminen V.-M., Maenhaut W., Jaffrezo J.-L., Balachandran S. & Davidson C.I. 1993. Size distributions of atmospheric trace elements at Dye 3, Greenland — I. Distribution characteristics and dry deposition velocities. *Atmos. Environ.* 27A: 2787–2802.
- IPCC 1995. Climate Change 1994, Radiative Forcing of Climate Change and An Evaluation of the IPCC IS92 Emission Scenarios. Report of the Intergovernmental Panel on Climate Change (IPCC), Cambridge University Press, Great Britain, 1995.

- Jaffrezo J.-L. & Davidson C.I. 1993. The Dye 3 gas and aerosol sampling program (DGASP): an overview. *Atmos. Environ.* 27A: 2703–2707.
- Kerminen V.-M. & Wexler A. 1995. The interdependence of aerosol processes and mixing in point source plumes. *Atmos. Environ.* 29: 361–375.
- Kerminen V.-M. & Wexler A. 1996. The occurrence of sulfuric acid — water nucleation in plumes: urban environment. *Tellus* 46B: 65–82.
- Kerminen V.-M., Aurela M., Hillamo R. and Virkkula A. 1997. Formation of particulate MSA — deductions from size distribution measurements in the Finnish Arctic. *Tellus* 49B: 159–171.
- Ogren J.A. 1995. A systematic approach to *in situ* observations of aerosol properties. In Charlson R.J. & Heintzenberg J. (eds.), *Aerosol Forcing of Climate*. Wiley.
- Ogren J.A. & Sheridan P.J. 1996. Vertical and horizontal variability of aerosol single scattering albedo and hemispheric backscatter fraction over the United States. In Kulmala M. & Wagner P.E. (eds.) *Nucleation and Atmospheric Aerosols, Proceedings of the Fourteenth International Conference on Nucleation and Atmospheric Aerosols*. Helsinki 26–30 August, 1996. Elsevier.
- Ottar B. 1989. Arctic air pollution: a Norwegian perspective. *Atmos. Environ.* 23: 2349–2356.
- Ottar B., Pacyna J.M. & Berg T.C. 1986. Aircraft measurements of air pollution on the Norwegian Arctic. *Atmos. Environ.* 20: 87–100.
- Pacyna J.M., Ottar B., Tomza U. & Maenhaut W. 1985. Long-range transport of trace elements to Ny-Ålesund, Spitsbergen. *Atmos. Environ.* 19: 857–865.
- Raatz W.E. & Shaw G.E. 1984. Long-range tropospheric transport of pollution aerosols into the Alaskan Arctic. *J. Climate App. Met.* 23: 1052–1064.
- Raatz W.E. 1991. The climatology and meteorology of Arctic air pollution. In Sturges W.T. (Ed.) *Pollution of the Arctic atmosphere*. Elsevier, London, pp.13–42.
- Salonjoja M. 1993. (*Real-time forecasting of long-range dispersion of a radioactive release caused by a severe nuclear accident*). M.Sc. Thesis, Helsinki University of Technology, Department of Technical Physics (in Finnish).
- Seibert P., Kromp-Kolb H., Baltensperger U., Jost D.T., Schikowski M., Kasper A. & Puxbaum H. 1994. Trajectory analysis of aerosol measurements at high alpine sites. In: Borrell P.M., Borrell P., Cvitač T. & Seiler W. (eds.), *Transport and transformation of pollutants in the troposphere*. Proceedings of EUROTRAC Symposium '94., Academic Publishing, Den Haag, pp.689–693.
- Seinfeld J.H. 1986. *Atmospheric chemistry and physics of Air pollution*. Wiley, New York.
- Stohl A. 1996. Trajectory statistics — a new method to establish source-receptor relationships of air pollutants and its application to the transport of particulate sulfate in Europe. *Atmos. Environ.* 30: 579–587.
- Stohl A., Wotawa G., Seibert P. & Kromp-Kolb H. 1995. Interpolation errors in wind fields as a function of spatial and temporal resolution and their impact on different types of kinematic trajectories. *J. Appl. Meteor.* 34: 2149–2165.
- Thielke J.F., Charlson R., Winter J. W., Ahlquist N. C., Whitby K. T., Husar R. B. & Liu B.Y.H. 1972. Multiwavelength nephelometer measurements in Los Angeles smog aerosols. II. Correlation with size distributions, volume concentrations. *J. Colloid Inter. Sci.* 39: 252–259
- Tikkanen E. & Niemelä I. (eds.) 1995. *Kola Peninsula pollutants and forest ecosystems in Lapland*. Final report of the Lapland Forest Damage Project. *Finnish Forest Research Institute*, Rovaniemi, Finland.
- Tuovinen J.-P., Laurila T., Lättilä H., Ryaboshapko A., Brukhanov P. & Korolev S. 1993. Impact of the sulphur dioxide sources in the Kola peninsula on air quality in northernmost Europe. *Atmos. Environ.* 27A: 1379–1395.
- Valkama I. & Rossi J. 1992. Description of the model TRADOS. In Klug W., Graziani G., Grippa G., Pierce D. & Tassone C. (eds.), *Evaluation of long range atmospheric transport models using environmental radioactivity data from the Chernobyl accident*. *The ATMES report*, Elsevier Publ.
- Valkama I. & Salonjoja M. 1993. (Operational long-range dispersion and dose model for radioactive releases). *Finnish Meteorological Institute, Helsinki*, (in Finnish).
- Valkama I., Salonjoja M., Toivonen H., Lahtinen J. & Pöllänen R. 1995. Transport of radioactive gases and particles in the Chernobyl accident: comparison of environmental measurements and dispersion calculations. Extended synopses of International Symposium on Environmental Impact of Radioactive Releases, Vienna, Austria, 8–12 May 1995. *IAEA-SM-339/69*.
- Virkkula A. 1997. Performance of a differential optical absorption spectrometer (DOAS) in surface ozone measurements in the Finnish Arctic. *Atmos. Environ.* 31: 545–555
- Virkkula A. and Hillamo R.E. 1995. Three-wavelength nephelometer measurements in the Finnish Arctic. *J. Aerosol Sci.* 26: S451–S452.
- Virkkula A., Mäkinen M., Hillamo R. & Stohl A. 1995. Atmospheric aerosol in the Finnish Arctic: particle number concentrations, chemical characteristics, and source analysis. *Water, Air, and Soil Poll.* 85: 1997–2002.
- Virkkula A., Mäkinen M., Hillamo R.E., Kerminen V.-M. & Stohl A. (1996). Physical properties and sources of atmospheric aerosol in the Finnish Arctic. *Proceedings of the Fourteenth International Conference on Nucleation and Atmospheric Aerosols, Helsinki 26–30 August, 1996* Elsevier. 593–598
- Waggoner A.P. & Weiss R.E. 1980. Comparison of fine particle mass concentration and light scattering extinction in ambient aerosol. *Atmos. Environ.* 14: 623–630.